The Successive-Order-of-Interaction Radiative Transfer Model. Part II: Model Performance and Applications

CHRISTOPHER W. O'DELL

Department of Atmospheric and Oceanic Sciences, University of Wisconsin—Madison, Madison, Wisconsin

ANDREW K. HEIDINGER

Advanced Satellite Products Branch, NOAA/NESDIS Office of Research and Applications, Madison, Wisconsin

THOMAS GREENWALD

Cooperative Institute for Meteorological Satellite Studies, University of Wisconsin—Madison, Madison, Wisconsin

PETER BAUER

European Centre for Medium-Range Weather Forecasts, Reading, United Kingdom

RALF BENNARTZ

Department of Atmospheric and Oceanic Sciences, University of Wisconsin—Madison, Madison, Wisconsin

(Manuscript received 9 March 2005, in final form 22 February 2006)

ABSTRACT

Radiative transfer models for scattering atmospheres that are accurate yet computationally efficient are required for many applications, such as data assimilation in numerical weather prediction. The successive-order-of-interaction (SOI) model is shown to satisfy these demands under a wide range of conditions. In particular, the model has an accuracy typically much better than 1 K for most microwave and submillimeter cases in precipitating atmospheres. Its speed is found to be comparable to or faster than the commonly used though less accurate Eddington model. An adjoint has been written for the model, and so Jacobian sensitivities can be quickly calculated. In addition to a conventional error assessment, the correlation between errors in different microwave channels is also characterized. These factors combine to make the SOI model an appealing candidate for many demanding applications, including data assimilation and optimal estimation, from microwave to thermal infrared wavelengths.

1. Introduction

There is currently a need for fast yet accurate radiative transfer (RT) models for scattering atmospheres. Numerical weather prediction (NWP) models rely increasingly on assimilation of radiance data directly, rather than on derived products (English et al. 2000). Operational centers are beginning to contemplate assimilating microwave and infrared radiances under all-weather conditions, instead of under clear skies only, as is currently done (Greenwald et al. 2002). For this assimilation to be feasible, both forward and adjoint radiative transfer codes are required, and these models must be very fast. For example, the European Centre for Medium-Range Weather Forecasts (ECMWF) has recently begun assimilation of microwave radiances in scattering atmospheres using an Eddington model (Bauer et al. 2004, 2006a,b). In addition to data assimilation, some retrieval algorithms are beginning to use ensemble-type approaches, wherein a large number of possible profiles with varying atmospheric parameters are forward modeled to produce top-of-atmosphere (TOA) radiances at various frequencies to find the best

Corresponding author address: Christopher W. O'Dell, Department of Atmospheric and Oceanic Sciences, University of Wisconsin—Madison, 1225 West Dayton St., Madison, WI 53706.
E-mail: odell@aos.wisc.edu

match with measurements (e.g., Evans et al. 1995; Skofronick-Jackson et al. 2004); often this is performed within the framework of optimal estimation (see e.g., Rodgers 2000). Many authors have presented RT models to meet some of these needs (e.g., Voronovich et al. 2004; Ou et al. 2004; Greenwald et al. 2005; Bauer et al. 1998).

In Heidinger et al. (2006, hereinafter Part I), we described the theoretical foundations for a one-dimensional, azimuthally symmetric radiative transfer model dubbed the "successive order of interaction" (SOI) model. This model is best described as a doubling–adding model without the adding, which is itself replaced by a successive-order-of-scattering approach (see, e.g., Irvine 1965; Greenwald et al. 2005). The model employs a variety of useful approximations to calculate TOA radiances or brightness temperatures (TB) quickly and accurately. This paper seeks to explore the characteristics of the SOI model relevant to data assimilation and related applications and is organized as follows. First, section 2 examines the performance of the model in terms of both speed and accuracy under a variety of conditions. Section 3 explores the error characteristics of the SOI model in more detail, including an examination of the correlation between errors in different channels, information that is necessary for some applications. Section 4 discusses the calculation of Jacobian sensitivities through a model adjoint, illustrated with an example relevant to NWP.

2. Performance of the SOI model

a. Model accuracy

For accuracy, a radiative transfer TB error of less than approximately 1 K is sufficient for many applications. However, with instrument errors approaching tenths of a kelvin in some situations, it is reasonable to aim for radiative transfer TBs of a similar or even better accuracy. As described in Part I, the parameters within the basic SOI approach largely determining speed and accuracy are the number of quadrature angles used, as well as the initial layer thickness employed in the doubling routine. Values of these parameters were chosen as a compromise between speed and accuracy, to maximize the usefulness of the model. To be specific, a two-stream model with a maximum initial layer optical thickness of 0.1 is employed for only mildly scattering profiles and a four-stream model with a maximum initial layer optical thickness of 0.01 is used for more strongly scattering profiles. The measure used to quantify the importance of scattering is the column scattering optical depth (CSOD), defined as the vertical integral of the scattering coefficient. The value of CSOD defining the cutoff between two and four streams is 10^{-2}. Both the accuracy and computational speed of the SOI model will be studied in the following sections.

1) RAIN PROFILES IN THE MICROWAVE

The SOI model was first tested for accuracy in the microwave regime for which it was originally designed. The test cases employed were the four rain profiles over ocean of Smith et al. (2002), at the frequencies 10.7, 18.7, 23.8, 36.5, and 89.0 GHz. Calculations were made for both nadir and 53.1° observation angles. Each profile prescribed the extinction, single-scatter albedo, asymmetry parameter, and temperature for each of 41 atmospheric layers. A Henyey–Greenstein phase function was assumed (Henyey and Greenstein 1941). The benchmark employed was the reverse Monte Carlo model of Petty (1994), run to an accuracy of 0.01 K.[1] A Monte Carlo was chosen as the benchmark because of its ability to simulate explicitly nearly all relevant processes in the problem, despite the relatively long computation time required to achieve the desired accuracy. The Monte Carlo calculations agreed with those of Roberti et al. (1994) to within 0.05 K for all cases. We compared the SOI model with the performance of both a two-stream Eddington model (Evans and Stephens 1990), and the doubling–adding model of Bauer and Schluessel (1993), hereinafter referred to as the DA model. The DA model employed eight-stream Gauss–Lobotto quadrature with linear interpolation to determine the upwelling brightness temperatures at the observation angles.

The results of the calculations for each of the four rain profiles are shown in Fig. 1. The SOI model displayed excellent accuracy overall for these cases; it had an RMS error of approximately 0.21 K (for all cases, frequencies, and angles tested), comparing similarly to the DA model which showed an RMS error of 0.32 K. The SOI model also performed well in terms of maximum error: it had an extreme error of 0.76 K, as compared with 0.95 K for the DA model. The Eddington model had considerably worse errors, with an RMS error about 4 times those of both of the other models and a maximum error of 1.86 K.

Given that the Eddington model is effectively a two-stream model, it performs admirably. However, it may seem surprising that the SOI model performs as well as the DA model. This result may be attributable to the

[1] That is, the Monte Carlo model was run repeatedly until the standard deviation of the results was less than 0.01 K.

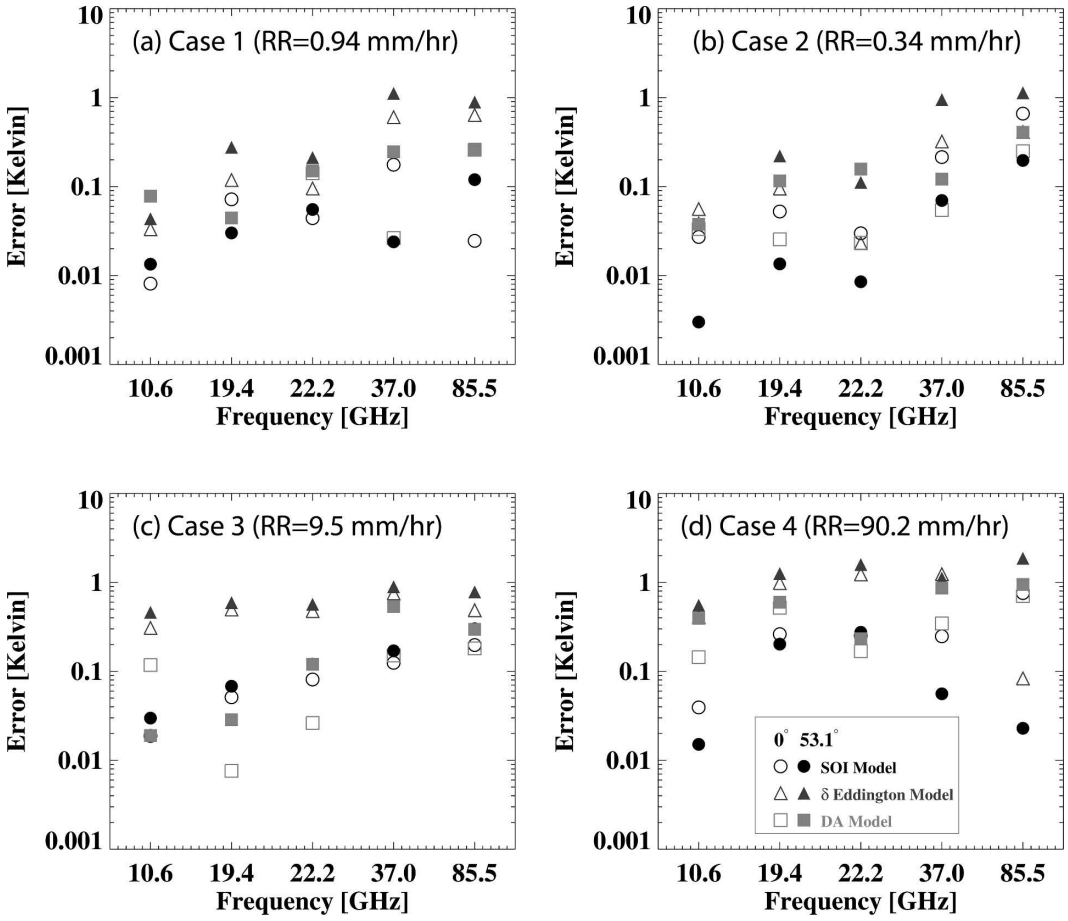

FIG. 1. The performance of several models in the microwave, for the Smith et al. (2002) rain profiles. All panels display the absolute value of the model error as a function of frequency for three models. The triangles represent the two-stream Eddington model, the squares represent the eight-stream DA model, and the circles represent the SOI model. The symbols are open for nadir incidence and are filled for 53.1° incidence. (a) Results for the low-water, low-ice-content profile; (b) low-water, high-ice-content profile; (c) high-water, low-ice-content profile; (d) high-water, high-ice-content profile. Corresponding rain rates are given in each panel. See Smith et al. (2002) for further details.

fact that the DA model does not have a stream set aside for the observation angle of interest (at least for the 53.1° cases), and so an interpolation must be done after the model is run to determine the brightness temperature at the observation angle. In general, we find that this technique is not as accurate as specifically including a stream at the observation angle with zero weight, a result found to be independent of the specific interpolation technique used. This is evident in Fig. 1, where the accuracy of the DA model for nadir incidence is clearly better than for 53.1° incidence.

2) SNOW PROFILES AT MILLIMETER WAVELENGTHS

Another possible area of applicability for the SOI model is at millimeter wavelengths. Snowfall detection from satellite platforms is thought to be feasible over both land and ocean, using frequencies in the range of roughly 80–400 GHz (Skofronick-Jackson et al. 2004). Ice water path and ice particle size retrievals may be feasible using frequencies from 180 to 900 GHz (Evans et al. 2002). For these types of retrievals, RT models are again needed that are both fast and accurate. To this end, we have tested the SOI model against the wintertime cases of Kim et al. (2004). In that study, the models tested were an Eddington model with and without δ scaling, and an iterative Neumann model (Irvine 1965) with and without the geometric series (GS) approximation. The benchmark used was a backward Monte Carlo model (Roberti et al. 1994).

For these tests, the same profiles of optical properties were used as were used by Kim et al. (2004), but as a benchmark the Monte Carlo of Petty (1994), run to an

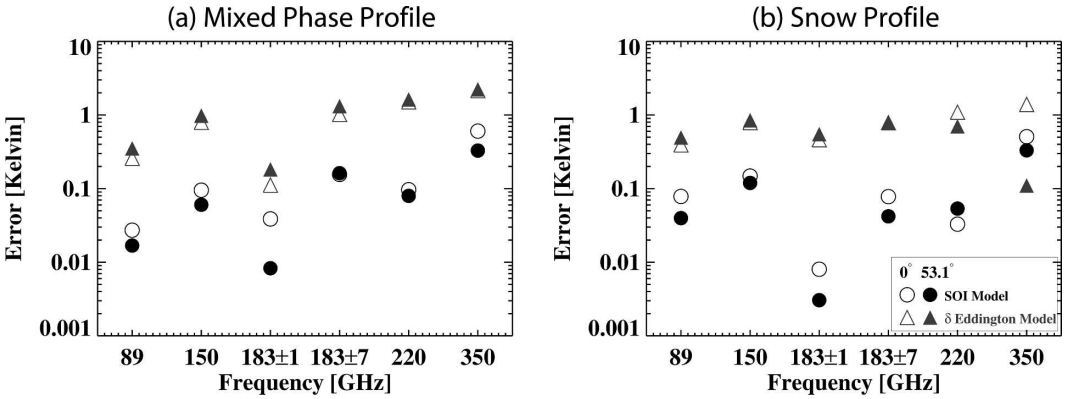

FIG. 2. The performance of the SOI and Eddington models at millimeter-wave frequencies, for two Kim et al. (2004) wintertime profiles for (a) mixed-phase (rain and snow) and (b) snow profiles. Both panels display the absolute value of the model error as a function of frequency. The triangles represent a two-stream Eddington model, and the circles represent the SOI model. The symbols are open for nadir incidence and are filled for 53.1° incidence.

accuracy of 0.01 K, was again employed. For comparison purposes, we tested both the SOI and Eddington models. The results of this comparison are shown in Fig. 2. In general, the SOI model is about 5 times as accurate as the Eddington model. For the eight frequencies tested (89, 119, 150, 183 ± 1, 183 ± 3, 183 ± 7, 220, and 350 GHz), the SOI model displayed an RMS accuracy of 0.15 K, with a maximum error of 0.60 K. The Eddington model in contrast had an RMS error of 0.76 K and a maximum error of 2.2 K. For all frequencies except 350 GHz (where there is the highest amount of scattering), the SOI model never had an error higher than 0.16 K, and it was typically about one order of magnitude more accurate than the Eddington model. These results are thus similar to those obtained for the Smith et al. (2002) microwave cases.

b. Model speed

In addition to accuracy, the issue of computation speed is an important characteristic for any radiative transfer model. In the context of data assimilation, it can be a crucial factor in deciding the model to be used. Table 1 shows the mean computation times per profile for both the Smith et al. (2002) and the Kim et al. (2004) cases. The SOI model is seen to be significantly faster than the Eddington model for the Smith et al. cases and has about the same speed for the Kim et al. cases. However, it should be noted that, as discussed in Part I, the SOI model simultaneously calculates both vertical and horizontal brightness temperatures while both the Eddington and DA models tested require one run per polarization. For applications requiring both polarizations, the computation time required for the Eddington model will be roughly 2 times as long as for the SOI model. Although they are not an exhaustive study of computation speed, from these studies we see that the speed of the SOI model is approximately the same as the operationally used Eddington model, and in some situations it is faster.

3. Radiative transfer error characteristics

The accuracy and speed of the SOI model as indicated in the previous section imply that it may make a good candidate model to be used in data assimilation or optimal estimation. For both of these applications, however, the model errors must be understood well. In particular, one must have estimates of not only the bias and variance of the model error, but also of the covariance. These quantities contribute to the observation error covariance matrix that appears in the mathematics of both data assimilation and optimal estimation (see, e.g., Rodgers 2000 and references therein). These variables must be assessed within the framework of a particular forward model, as well as for a particular set of sensors and for each different source of error. The problem is therefore extensive and complex, and we cannot completely and generally characterize these error properties for the SOI model. However, in this section we will analyze these error characteristics for a

TABLE 1. Model speeds for two case studies.

Model	Smith et al. (2002) computation time	Kim et al. (2004) computation time
Eddington	225 μs	134 μs
SOI	100 μs	136 μs
DA	8.8 ms	Not tested

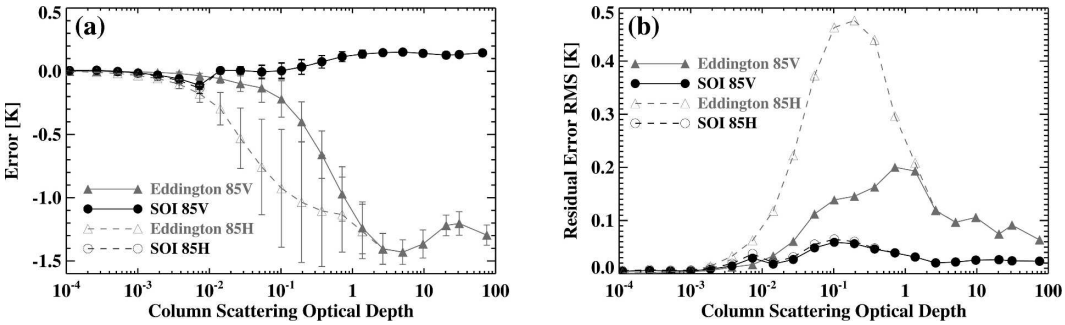

FIG. 3. The (a) radiative transfer errors and (b) standard deviation of those errors of the SOI and Eddington models, as performed on 12 970 atmospheric profiles chosen for their variability of precipitation, for the SSM/I 85.5-GHz *V* and *H* channels. Both quantities are displayed as a function of the column-scattering optical depth. Calculations were performed assuming the SSM/I observation angle of 53.1°. In (a), the vertical error represent $\pm 1\sigma$ of the results.

realistic example that not only will give an idea of the magnitude and general behavior of these quantities for one particular error source, but will also illustrate the basic steps necessary to such an analysis.

a. One-dimensional model errors

There are many possible sources of forward model error, such as from microphysics approximations, approximations in the surface emission and reflection, and various error sources in the radiative transfer itself. The details of the application in question will often determine the most important error source. The errors in the SOI model described in section 2, resulting from errors in doubling, discretization of the angular radiation field, and so on, we term one-dimensional (1D) model errors. These errors were found to be less than a few tenths of a kelvin for all cases studied for the SOI model and on the order of or less than a kelvin for the Eddington model. Although this level of error is greater than typical sensor noise, it is usually the smallest source of model error, and thus 1D model errors can often be neglected. For the sake of completeness, however, we present an example of these error statistics here. We draw our example from the ECMWF efforts to assimilate cloudy and precipitating radiances from several Special Sensor Microwave Imager (SSM/I) channels aboard the U.S. Defense Meteorological Satellite Program satellites (Bauer et al. 2006a,b). The SSM/I has seven microwave channels at the frequencies of 19.35, 22.235, 37.0, and 85.5 GHz; except for 22.235 GHz, each band has separate channels for both vertical and horizontal polarizations (Hollinger et al. 1987). The study includes 12 970 atmospheric profiles generated from the ECMWF global NWP model, chosen for their strong precipitation in terms of both rain and snow content (see Bauer et al. 2006c for details). All profiles consisted of 60 atmospheric layers. The profiles were taken from both tropical and extratropical areas, from forecasts in both July and December. Profiles of pressure, temperature, water vapor, cloud liquid water, and cloud ice were used to obtain absorption coefficients for each layer using the algorithms of Rosenkranz (1998) and Liebe et al. (1991). Profiles of rain and snow rates were converted to optical properties of extinction, single-scatter albedo, and asymmetry parameter using the precipitation microphysics model of Bennartz and Petty (2001). The lower surface was taken to be ocean, with emissivity calculated using version 2 of the Fast Emissivity Model (FASTEM-2) ocean surface emissivity model (Deblonde and English 2001).

Because ECMWF employs the Eddington model for its radiative transfer, we assess the error characteristics of both the Eddington and SOI models for this example. The reference model was an adding–doubling model with 32 streams employing Gauss–Legendre quadrature, distinct from the eight-stream DA model of section 2a(1). This model was chosen over the Monte Carlo model as the reference because the latter was too slow for these tests. However, the reference model was compared with the Monte Carlo model for consistency; agreement was found to be better than 0.05 K for all cases tested. Figure 3a shows the errors for both the Eddington and SOI models at 85.5 GHz as a function of CSOD. The error bars shown in the figure represent ± 1 standard deviation of the range of errors in each CSOD bin. It is seen that the errors from both models are relatively small, less than approximately 1.5 K for the Eddington model and less than 0.2 K for the SOI model; both are generally worse for higher CSOD. Also, we see that these errors are somewhat correlated with CSOD, leading to a rough model bias as a function of CSOD. It is a simple matter to remove this empiri-

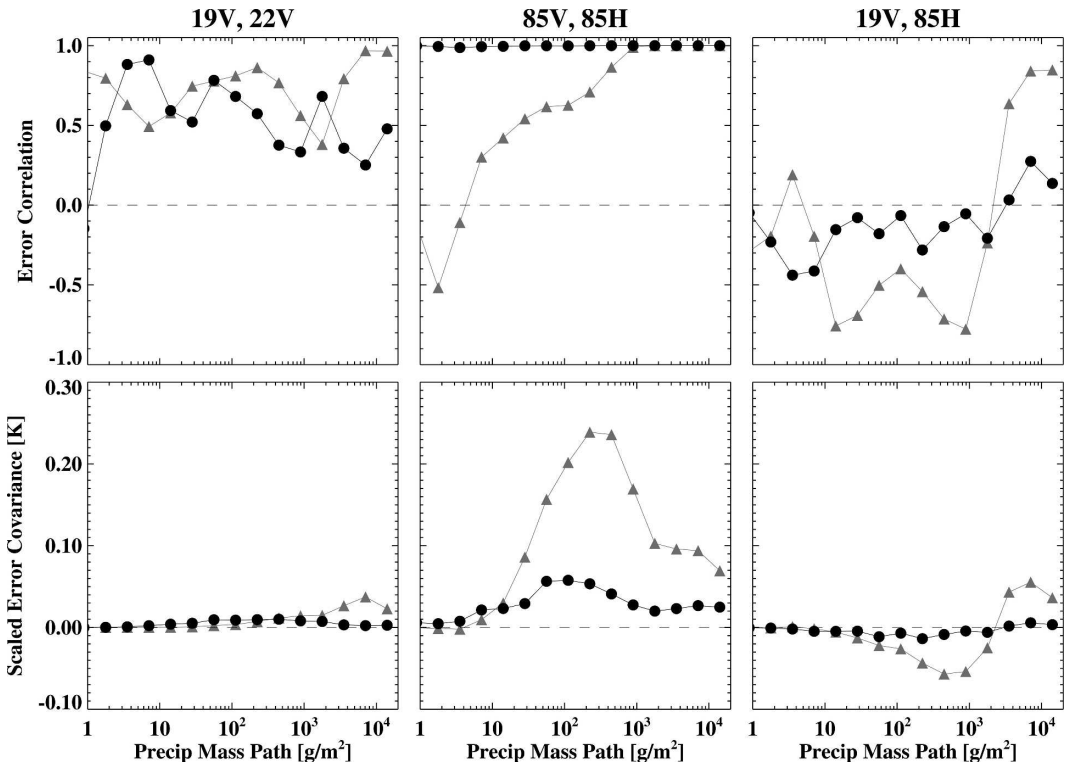

FIG. 4. Error correlation and scaled error covariance for selected SSM/I channel combinations plotted as a function of precipitation mass path for both the Eddington (gray triangles) and SOI (black circles) models. The scaled error covariance is a simple function of the error covariance, as defined in the text.

cally-determined mean bias as a function of CSOD; we used a cubic-spline interpolation between the CSOD bins shown in Fig. 3.

Once the bias removal is performed, each RT model is then roughly bias free (for this frequency, model and observation angle). The RMS errors of the bias-removed models are plotted in Fig. 3b and are consistent with the error bars in Fig. 3a. The RMS of the residuals is seen to be very modest, less than roughly 0.5 K for the Eddington model and less than 0.1 K for the SOI model. Errors were smaller, to varying degrees, for the other frequencies tested. Because of the small error magnitude, other sources of errors will often dominate the observation error covariance matrix for most applications. However, it is a useful exercise to evaluate these error covariances nonetheless. Because the SSM/I has seven channels as described above, the full observation error covariance is represented by a 7×7 symmetric matrix; this implicitly assumes that observations for different pixels can be treated as independent. The observation error covariance matrix contains contributions from *all* error sources, such as microphysics error, radiative transfer error, errors resulting from cloud overlap assumptions, and sensor noise. The error covariance between two channels j and k, given a set of model errors for each channel, is given by

$$s_{jk}^2 = \mathrm{var}(j, k) = \frac{1}{N-1} \sum_{i=1}^{N} \epsilon_{i,j} \epsilon_{i,k}, \tag{1}$$

where $\epsilon_{i,j}$ is the model error for channel j and data point i. Note that s_{jk}^2 may be positive or negative. The covariance of two channels is related to the correlation r_{jk} between their errors in the usual manner:

$$r_{jk} = \frac{s_{jk}^2}{s_j s_k}, \tag{2}$$

where s_j and s_k are the standard deviations of the errors for channels j and k, respectively.

The error correlations and covariances are displayed in Fig. 4 for three selected channel combinations, plotted as a function of the precipitation mass path. This quantity is used as the independent variable because it is roughly proportional to CSOD for each frequency tested but is itself independent of frequency. Instead of plotting the error covariance (which has units of kelvins squared), we instead plot the scaled error covariance given by $\pm(|s_{jk}^2|)^{1/2}$, where the sign matches that of the actual covariance. The first channel combination shown

is 19*V* with 22*V* (*V* denotes vertical polarization). Because both of these frequencies are generally sensitive to similar atmospheric variables, we expect their errors to be somewhat correlated. This is indeed true for both models tested, with correlations around 50% for the SOI model and around 70% for the Eddington model. Because of their low RMS errors, however, the overall covariances are very low, less than 0.05 K. The next channel combination shows the error correlations of two extremely similar channels, 85*V* and 85*H* (*H* denotes horizontal polarization). Though the SOI model shows nearly perfectly correlated errors, as one might expect, correlations from the Eddington model exhibit a more complicated behavior. For higher amounts of precipitation, the two errors are highly correlated, but the correlation is lower for smaller amounts of precipitation. This is most likely a surface effect, resulting from the simplified treatment of the surface emissivity in the Eddington model. The final channel combination shows two more dissimilar channels, 19*V* with 85*H*. Both models show a somewhat complicated behavior, going from negative correlation for smaller mass paths to positive correlation for higher mass paths, though this trend is much more pronounced for the Eddington model. The behavior of the covariances reflects this.

The behavior of the various covariances is thus not necessarily easy to guess, based on the known assumptions in the models themselves. Also, it is likely that some of these behaviors are related to the specifics of this particular example and implementation. For instance, the use of a different microphysics model or surface emissivity model could in principle lead to different covariances among radiative transfer errors. It must therefore be stressed that this kind of analysis must always be carried out on a representative dataset and using the same set of forward models that the application in question will itself use.

b. Other sources of error

Several other sources of error exist for the SOI and other radiative transfer models that can possibly lead to nonnegligible forward-model error. As stated previously, some of these error sources can lead to much larger errors than the 1D errors described above, and as such these error sources must also be characterized in terms of bias and covariance for applications such as data assimilation or optimal estimation.

The common step of approximating the phase function as Henyey–Greenstein (Henyey and Greenstein 1941) can lead to errors, especially for low-asymmetry parameters when the phase function is typically Rayleigh in shape rather than isotropic. Although technically a 1D error, we separate this effect from the others because of the widespread employment of this approximation. It is of course often possible to use the expansion coefficients of the phase function directly in the radiative transfer model, rather than simply the asymmetry parameter. This is in principle possible for the SOI model, but errors resulting from this assumption have yet to be analyzed in detail.

An important source of RT error for coarse-resolution models is that due to cloud overlap assumptions. Coarse model profiles often contain subgrid-scale variability that is parameterized in terms of a cloud-cover fraction. To simulate radiances from an individual atmospheric profile accurately, multiple radiative transfer calculations may be necessary. Bauer et al. (2006c) find that these errors can be tens of kelvin, with biases of a few kelvin, for precipitating profiles at certain microwave frequencies. That study proposes a useful bias removal but does not characterize the covariance of the resulting errors. For higher-resolution regional-scale models, the analogous source of error is the neglect of the three-dimensional nature of the RT problem, leading to what are often called "3D errors." Several authors have explored the magnitude of this error source in the microwave context (Roberti et al. 1994; Liu et al. 1996; Bauer et al. 1998). Studies performed with the SOI model on hurricane simulations with a regional model have found that these errors can be many tens of kelvin but can be greatly reduced by the use of a "slant path" one-dimensional model, a finding that is in accordance with previous studies (both the slant-path and plane-parallel versions of the SOI model were available online at http://naftali.aos.wisc.edu/soi at the time of writing). However, as yet these 3D errors also have not been characterized in terms of bias, variance, and covariance.

4. Jacobian calculations

In addition to accurate characterization of forward-model errors, for applications involving either data assimilation or optimal estimation, Jacobian sensitivities of the modeled radiances with respect to optical and surface properties must typically be calculated (see, e.g., Thepaut and Moll 1990). For a model with many more inputs than outputs, such as a radiative transfer model, the fastest way to calculate these sensitivities is with an *adjoint* model (Giering and Kaminski 1998). An adjoint has been written for the SOI model, using standard techniques (Errico 1997; Giering and Kaminski 1998). For an introduction to adjoints and their construction, the reader is referred to Giering and Kaminski (1998).

A standard procedure to test the accuracy of a numerical adjoint is to compare its results with those of a

linearized version of the model in question, often called the "tangent-linear model." This is because the tangent-linear model should produce identical sensitivities as the adjoint model, though they operate on different principles. When this test was applied to the SOI model, its adjoint was found to agree with the linearized code to within machine-level accuracy. The adjoint is also relatively fast, being slower by only a factor of approximately 3–5 than the forward model itself for the Smith et al. (2002) cases. To illustrate the use of the adjoint, the forward and adjoint code have been run on a 12-h model forecast from the National Centers for Environmental Prediction Global Forecasting System (GFS), corresponding to 1200 UTC 21 September 2004. The same algorithms described in section 3a were used to generate layer optical and surface properties from the GFS output variables, with one small difference. Because only 6-h precipitation averages were available from the GFS model output, simple assumptions were made to obtain profiles of liquid and frozen precipitation rates; for further details, see Greenwald et al. (2005).

Figure 5a shows the modeled brightness temperatures for this day and time at 89 GHz across the North Atlantic, for 55.2° observation angle and horizontal polarization.[2] Hurricanes Jeanne and Karl are both apparent; on this day, Karl (centered at roughly 22° lat, −47° lon) was classified as a category-4 hurricane. The modeled values of TB compare well to corresponding measurements from the Advanced Microwave Scanning Radiometer for the Earth Observing System (AMSR-E) aboard the *Aqua* satellite (Fig. 5b); primarily this is due to correctly capturing the water vapor structure. Figure 5c shows the sensitivity of TB_H to changes in surface temperature, computed using the SOI adjoint model. It may seem counterintuitive that some sensitivities are negative, but this result is due to the fact that the surface emissivity has a negative dependence on temperature, and this indirect effect can overcome the direct effect that increasing the surface temperature has on the upwelling radiance at the surface; for a more detailed discussion, see Petty and Katsaros (1994). In a similar way, the sensitivity with respect to surface wind speed is shown in Fig. 5d, which is primarily due to the dependence of surface emissivity on wind speed. Of course, the sensitivities to surface characteristics are moderated by the surface-to-space transmission.

Figures 5e–h show the cross sections of the sensitivity of TB_H with respect to various atmospheric variables at −47° longitude (dotted line in Fig. 5a). Each sensitivity is defined such that a unit change in the variable of interest over one vertical kilometer of atmosphere yields that amount of change in TOA brightness temperature. Figure 5e displays the sensitivity to the volume-scattering coefficient k_s. This sensitivity is large and negative at locations high in the atmosphere and over the storm activity, because increasing the scattering there increases the fraction of cold space radiation reflected by the atmosphere into the sensor, thereby lowering the received brightness temperature. Near the surface, the dependence on k_s can sometimes be positive; this occurs primarily for view angles near zenith, where increasing the amount of scattering *increases* the fraction of radiation reflected into the viewing angle from more oblique angles. These more oblique angles tend to contain warmer downwelling radiation and hence can overcome the deficit incurred from reflecting more cold space radiation into the sensor.

Figure 5f likewise shows the sensitivity of TB_H to the volume absorption coefficient k_a. This quantity is almost always positive because of the fact that increasing absorption in the atmosphere also increases emission by the atmosphere, which is typically warmer in the microwave than the underlying ocean surface. However, $\partial TB/\partial k_a$ can also be negative, in particular in regions higher in the atmosphere overlying warmer emitting regions (Voronovich et al. 2004). The sensitivity to the asymmetry parameter (Fig. 5g) is similarly almost always positive, because increasing the amount of forward scattering reduces the contribution of the cold microwave background to the TOA brightness temperature relative to all other temperature sources. However, there are some instances in which sensitivity to the asymmetry parameter can in fact be negative—in particular, for very oblique viewing angles. Last, the sensitivity to the atmospheric temperature (Fig. 5h) is always nonnegative; these sensitivities are equivalent to the more commonly discussed weighting function. Note that this conclusion assumes that the optical properties are held constant while the atmospheric temperature of one model layer is allowed to change. In reality, the optical properties of the atmosphere often change as a result of a change in temperature, and this can cause the sensitivity of TB with respect to atmospheric temperature to be negative.

5. Discussion

The SOI radiative transfer model has been shown to be both fast and accurate in the microwave and submil-

[2] Horizontal polarization was chosen because the sensitivities of brightness temperature with respect to any atmospheric variables are greater than those for vertical polarization over nonopaque regions. When the sky is opaque, polarization is largely irrelevant.

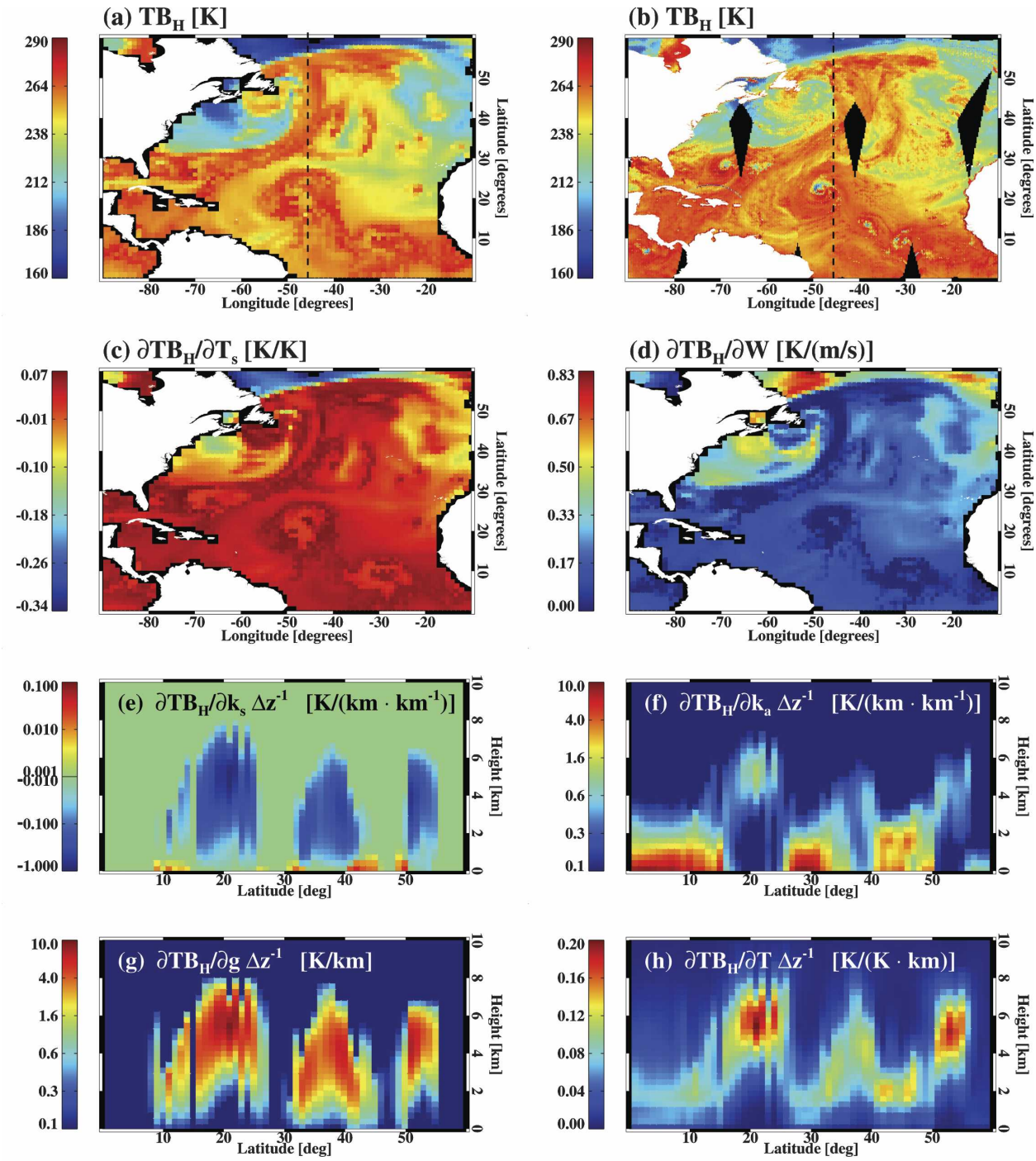

FIG. 5. (a) The 89-GHz (*H* polarization) modeled TOA brightness temperatures TB_H from a GFS simulation of 21 Sep 2004 (1200 UTC), at 55.2° incidence. (b) Corresponding observations from the AMSR-E satellite, taken over the day from 0348 to 1824 UTC. The sensitivity of TB_H to changes in (c) surface temperature T_s and (d) surface wind speed W is shown. Jacobian sensitivities to the atmospheric variables (e) volume scattering coefficient, (f) volume absorption coefficient, (g) asymmetry parameter, and (h) temperature are also shown. The Jacobian units employed for the atmospheric variables are such that a change of one unit of the variable in question over 1 km of height will yield a change of that many kelvins in TB.

limeter tests presented here. Its speed is comparable to or faster than the commonly used Eddington RT model, and its accuracy is typically better than 0.3 K at these wavelengths. The errors were also characterized in terms of bias, variance, and covariance for a specific microwave application. Though the 1D errors are very low, nearly identical analyses are required for other error sources particular to specific applications; this should be the subject of future study. Last, a fast adjoint for the SOI model has been created such that Jacobian sensitivities of atmospheric variables can be calculated. These properties make the SOI model a good candidate for use in data assimilation for NWP as well as applications employing optimal estimation.

The SOI model should also be useful in the infrared under cloudy conditions. Preliminary studies suggest that the number of orders of interaction needed in most cases is small, typically less than 10, and the ability to accept the full phase function could prove to be valuable. Because errors in the scattering coefficients themselves typically lead to errors in the final brightness temperatures of greater than 0.5 K, neglecting polarization, the burden of radiative transfer research from the microwave to the infrared is now largely upon the microphysics models to model the scattering properties of ice crystals and frozen hydrometeors more accurately.

Acknowledgments. This work was supported by the Joint Center for Satellite Data Assimilation through NOAA Cooperative Agreement NA07EC0676. Thanks are given to Min-Jeong Kim of NASA/GSFC for providing the optical properties for the millimeter-wave studies and to Grant Petty of the University of Wisconsin—Madison for several valuable discussions and for providing his Monte Carlo code.

REFERENCES

Bauer, P., and P. Schluessel, 1993: Rainfall, total water, ice water and water-vapor over sea from polarized microwave simulations. *J. Geophys. Res.,* **98,** 2757–2765.

——, L. Schanz, and L. Roberti, 1998: Correction of three-dimensional effects for passive microwave retrievals of convective precipitation. *J. Appl. Meteor.,* **37,** 1619–1632.

——, P. Lopez, A. Benedetti, E. Moreau, D. Salmond, and M. Bonazzola, 2004: Assimilation of satellite-derived precipitation information at ECMWF in preparation of a future European contribution to GPM (EGPM). ECWMF Internal Rep. 17193, 85 pp.

——, ——, ——, D. Salmond, and E. Moreau, 2006a: Implementation of 1D+4D-Var assimilation of precipitation-affected microwave radiances at ECMWF. Part, I, 1D-Var. *Quart. J. Roy. Meteor. Soc.,* in press.

——, ——, ——, ——, S. Saarinen, and M. Bonazzola, 2006b: Implementation of 1D+4D-Var assimilation of precipitation-affected microwave radiances at ECMWF. Part II: 4D-Var. *Quart. J. Roy. Meteor. Soc.,* in press.

——, E. Moreau, F. Chevallier, and U. O'Keefe, 2006c: Multiple-scattering microwave radiative transfer for data assimilation applications. *Quart. J. Roy. Meteor. Soc.,* **132,** 1259–1281.

Bennartz, R., and G. P. Petty, 2001: The sensitivity of passive microwave radiances in precipitating clouds to ice particle size distributions. *J. Appl. Meteor.,* **40,** 345–364.

Deblonde, G., and S. J. English, 2001: Evaluation of the FASTEM-2 fast microwave oceanic surface emissivity model. *Tech. Proc. ITSC-XI,* Budapest, Hungary, WMO and Co-sponsors, 67–78.

English, S. J., R. J. Renshaw, P. C. Dibben, A. J. Smith, P. J. Rayer, F. W. Saunders, and J. Eyre, 2000: A comparison of the impact of TOVS and ATOVS satellite sounding data on the accuracy of numerical weather forecasts. *Quart. J. Roy. Meteor. Soc.,* **126,** 2911–2931.

Errico, R., 1997: What is an adjoint model? *Bull. Amer. Meteor. Soc.,* **78,** 2577–2591.

Evans, K. F., and G. L. Stephens, 1990: Polarized microwave radiative transfer modeling: An application to microwave remote sensing of precipitation. Department of Atmospheric Sciences, Colorado State University, Paper 461, 79 pp.

——, J. Turk, T. Wong, and G. L. Stephens, 1995: A Bayesian approach to microwave precipitation profile retrieval. *J. Appl. Meteor.,* **34,** 260–279.

——, S. J. Walter, A. J. Heymsfield, and G. M. McFarquhar, 2002: Submillimeter-wave cloud ice radiometer: Simulations of retrieval algorithm performance. *J. Geophys. Res.,* **107,** 4028, doi:10.1029/2001JD000709.

Giering, R., and T. Kaminski, 1998: Recipes for adjoint code construction. *ACM Trans. Math. Software,* **24,** 437–474.

Greenwald, T. J., R. Hertenstein, and T. Vukicevic, 2002: An all-weather observational operator for radiance data assimilation with mesoscale forecast models. *Mon. Wea. Rev.,* **130,** 1882–1897.

——, R. Bennartz, C. W. O'Dell, and A. Heidinger, 2005: Fast computation of microwave radiances for data assimilation using the successive order of scattering approximation. *J. Appl. Meteor.,* **44,** 960–966.

Heidinger, A., C. W. O'Dell, T. Greenwald, and R. Bennartz, 2006: The successive-order-of-interaction radiative transfer model. Part I: Model development. *J. Appl. Meteor. Climatol.,* **45,** 1388–1402.

Henyey, L. C., and J. L. Greenstein, 1941: Diffuse radiation in the galaxy. *Astrophys. J.,* **93,** 70–83.

Hollinger, J. P., J. L. Pierce, and G. A. Poe, 1987: SSM/I instrument evaluation. *IEEE Trans. Geosci. Remote Sens.,* **28,** 781–790.

Irvine, W. M., 1965: Multiple scattering by large particles. *Astrophys. J.,* **142,** 1563–1575.

Kim, M. J., G. Skofronick-Jackson, and J. A. Weinman, 2004: Intercomparison of millimeter-wave radiation transfer models. *IEEE Trans. Geosci. Remote Sens.,* **42,** 1882–1890.

Liebe, H. J., G. A. Hufford, and T. Manabe, 1991: A model for the complex permittivity of water at frequencies below 1 THz. *Int. J. Infrared Millimeter Waves,* **12,** 659–675.

Liu, Q., C. Simmer, and E. Ruprecht, 1996: Three-dimensional radiative transfer effects of clouds in the microwave spectral range. *J. Geophys. Res.,* **101,** 4289–4298.

Ou, S. C., K. N. Liou, Y. Takano, E. Wong, K. D. Hutchison, and T. K. Samec, 2004: Comparison of the UCLA-LBLE radiative transfer model and MODTRAN for accuracy assessment

of the NPOESS-VIIRS cloud optical property algorithms. *Weather and Environmental Satellites,* T. H. Vonder Haar and H.-L. A. Huang, Eds., International Society for Optical Engineering (SPIE Proceedings Vol. 5549), 80–89.

Petty, G. W., 1994: Physical retrievals of over-ocean rain rate from multichannel microwave imagery. Part I: Theoretical characteristics of normalized polarization and scattering indices. *Meteor. Atmos. Phys.,* **54,** 89–100.

——, and K. B. Katsaros, 1994: The response of the SSM/I to the marine environment. Part II: A parameterization of the effect of the sea surface slope distribution on emission and reflection. *J. Atmos. Oceanic Technol.,* **11,** 617–628.

Roberti, L., J. Haferman, and C. D. Kummerow, 1994: Microwave radiative transfer through horizontally inhomogeneous precipitating clouds. *J. Geophys. Res.,* **99,** 16 707–16 718.

Rodgers, C. D., 2000: *Inverse Methods for Atmospheric Sounding*. World Scientific, 256 pp.

Rosenkranz, P. W., 1998: Water vapor microwave continuum absorption: A comparison of measurements and models. *Radio Sci.,* **33,** 919–928.

Skofronick-Jackson, G., M.-J. Kim, J. A. Weinman, and D.-E. Chang, 2004: A physical model to determine snowfall over land by microwave radiometry. *IEEE Trans. Geosci. Remote Sens.,* **42,** 1047–1058.

Smith, E. A., P. Bauer, F. S. Marzano, C. D. Kummerow, D. McKague, A. Mugnai, and G. Panegrossi, 2002: Intercomparison of microwave radiative transfer models for precipitating clouds. *IEEE Trans. Geosci. Remote Sens.,* **40,** 541–549.

Thepaut, J. N., and P. Moll, 1990: Variational inversion of simulated TOVS radiances using the adjoint technique. *Quart. J. Roy. Meteor. Soc.,* **116,** 1425–1448.

Voronovich, A. G., A. J. Gasiewski, and B. L. Weber, 2004: A fast multistream scattering-based Jacobian for microwave radiance assimilation. *IEEE Trans. Geosci. Remote Sens.,* **42,** 1749–1761.